



Temperature dependence of CIGS and perovskite solar cell performance: an overview

Leqi Lin¹ · N. M. Ravindra² Received: 12 March 2020 / Accepted: 2 July 2020 / Published online: 10 July 2020
© Springer Nature Switzerland AG 2020

Abstract

CIGS, with a tailorable direct band gap (of 1.04–1.68 eV), can serve as bottom cell with excellent band gap match with perovskite (1.6–2.3 eV) in the combined monolithic perovskite/CIGS tandem solar cell, that has the potential to exceed the Shockley–Queisser limit. Thus, an investigation of the operating temperature dependence of the performance of CIGS and perovskite solar cells (PSCs), in the temperature range of 80–380 K, based on studies in the literature, is presented. Besides the operating temperature, the influence of substrate temperature of CIGS solar cells, fabricated on soda-lime-glass, polyimide foil and stainless steel substrates are also investigated. The solar cell performance is assessed by considering several photovoltaic parameters such as short circuit current density (J_{sc}), open circuit voltage (V_{oc}), fill factor and power conversion efficiency. By a detailed understanding of the dependence of solar cell parameters on temperature for CIGS solar cells and PSCs, with different characteristics or structures, it is anticipated that an effective pathway for the improvement in these cells, in adverse environments, can be accomplished.

Keywords Solar cells · CIGS · Perovskite solar cells · Temperature dependence

1 Introduction

Today, from the perspective of photovoltaics, perovskites represent one of the most successful optoelectronic candidates with significant growth in their performance since 2009; they play a critical role in the next-generation solar cells for both terrestrial and space applications. Further, CIGS holds a market share of 21% of the total global thin film production among two other major materials, CdTe (76%) and a-Si (3%) according to the Photovoltaic Report by Fraunhofer Institute for Solar Energy Systems, ISE [1] (based on CIGS, CdTe and a-Si as the principal thin-film solar cell materials). Thin film solar cells [2] continue to enhance their role as high efficiency, reliable and cost-effective alternative to conventional mono-crystalline silicon solar cells due to their lower material costs, rising

efficiencies and ease of fabrication. Furthermore, thin-film solar cells have significant potential and critical advantages in sunbelt countries with better temperature coefficients and ideal power conversion efficiencies (PCE) in adverse environments over crystalline silicon solar cells [3]. The fundamental equations governing the performance of solar cells have been described in a large number of studies in the literature. In a previous study, Singh and Ravindra [4] have investigated the temperature dependence of Si, Ge, GaAs, InP, CdTe and CdS solar cells. The first studies of the comparison of solar cell efficiency versus E_g for various semiconductors, in the temperature range of 273–673 K, by Wysocki and Rappaport, were reported 60 years ago [5]. It is interesting and relevant to note that while there have been significant improvements in solar cell materials and device technology, not much has changed relative to the

✉ N. M. Ravindra, n.m.ravindra@njit.edu; nmravindra@gmail.com | ¹Department of Civil and Environmental Engineering, New Jersey Institute of Technology, Newark, NJ, USA. ²Interdisciplinary Program in Materials Science and Engineering, New Jersey Institute of Technology, Newark, NJ, USA.



absolute solar cell efficiencies as function of materials and temperature. The temperature dependence of the bandgap (E_g) of semiconductors is described by the well-known Varshni relation [6] in Eq. (1), where $E_g(T)$ is the bandgap of the semiconductor at temperature T , $E_g(0)$ is its value at 0 K, and α and β are constants that are material dependent.

$$E_g(T) = E_g(0) - \frac{\alpha T^2}{(T + \beta)} \quad (1)$$

Since the first report of CIGS solar cells by Devaney and Mickelsen in 1987 [7], the technology has grown over the years; the best record efficiency of CIGS solar cells of 22.9% has been reported by Solar Frontier on glass substrates [8]. Normally, the structure of CIGS solar cell starts with soda-lime glass (SLG) substrate and Mo back contact on the bottom, followed by CIGS as the interlayer, on the top are ZnO/Al:ZnO and n-type CdS as window layer, and it is usually fabricated by a co-evaporation process and precursor reaction process. The cross section of a typical CIGS solar cell is as shown in Fig. 1a. The emerging thin film material solar cells, perovskite solar cells (PSCs), have also attracted increasing scientific and technological interest because of their high efficiency that can be attributed to their ability to fulfill the multiple roles of light-absorption, charge separation, transportation of holes and electrons in materials [9]; additionally, they offer the benefit of the use of low amounts of earth abundant materials. PSCs, based on either mesoscopic or planar, normal (n-i-p) or inverted (p-i-n) structure architectures, are typically described by the formula ABX_3 , where X is a halide anion, A is an organic

and/or inorganic cation, such as MA (methylammonium cation (CH_3NH_3^+)), FA (formamidinium ($\text{CH}(\text{NH}_2)_2^+$)), Cs and Rb and B is metal cation such as Pb (A being larger than B). The cross section of a typical perovskite solar cell is as shown in Fig. 1b [10]. Since the first report of PSCs with 3.8% power conversion efficiency (PCE) by Kojima et al. in 2009 [11], the organometal halide PSCs have been demonstrated with high PCE of > 23% on a lab-scale [12]. Enhanced light harvesting by using two or more absorbers, with different band gaps, has so far been the most effective approach to increase the PCE from 20 to over 30% beyond the practical limits of single p-n junctions. Conventionally, the low PCE of tandem device is primarily limited by the low efficiency and non-ideal bandgap of the top structure of the cells. This situation has changed with the advent of perovskite solar cells with wide and tunable band gap over a broad energy range [13]. Perovskite materials are, in most cases, direct-bandgap semiconductors with a bandgap ranging across the entire visible spectrum [14]. Among various kinds of tandem cells, perovskite/CIGS thin-film tandem cells hold great promise as each single junction cell has attained > 23% efficiency [15] and the bandgaps of both absorbers can be easily tailored for current matching conditions [16].

The study of the behavior of solar cells with temperature (T) is important as, in the working condition, they are generally exposed to temperatures ranging from 288 to 323 K [17] and to even higher temperatures in space and concentrator systems (370–380 K) [18]. The performance of solar cells is determined by the photovoltaic (PV) parameters, for example, short circuit current density (J_{sc}), open

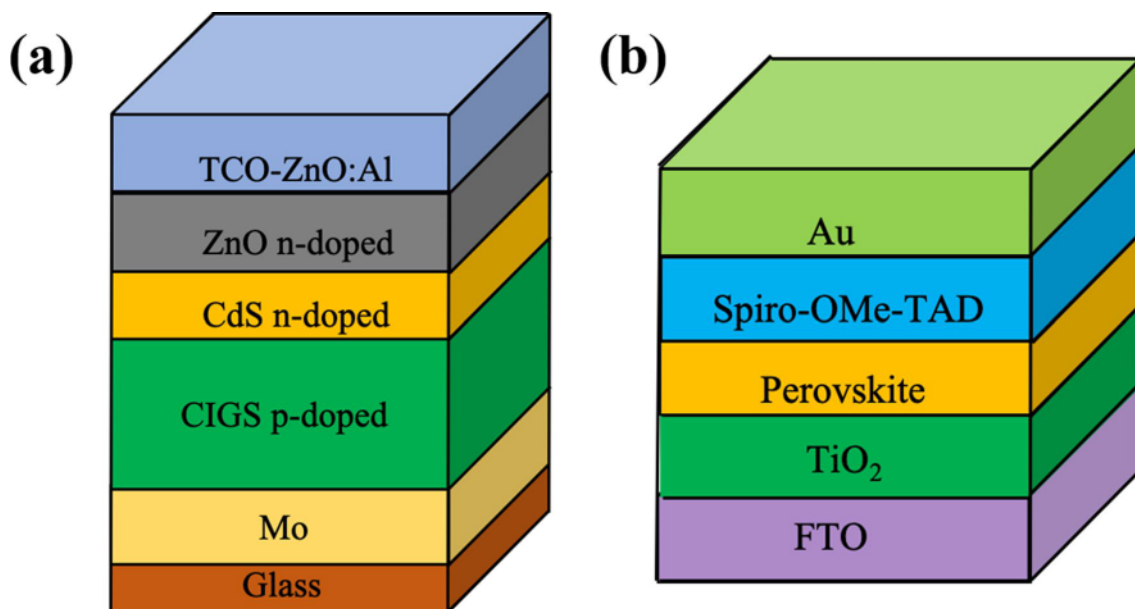


Fig. 1 Cross section of **a** a typical CIGS solar cell, **b** perovskite solar cell

circuit voltage (V_{oc}), fill factor (FF) and PCE. These parameters are temperature-dependent and hence affect the performance of solar cells [4]. In general, V_{oc} decreases with increasing temperature and J_{sc} increases slightly with increasing temperature [4]. Both FF and PCE decrease with increasing temperature and PCE degradation is mainly due to the decrease in V_{oc} [4]. The temperature-related studies will be important for further improvement in performance of these PV cells. In the first section, this paper presents a review of the dependence of PV parameters of CIGS solar cells on operating temperatures and substrate temperatures (T_{sub}). The substrate has a crucial role in determining the PCE performance of the whole device. The operating temperature dependence of PV parameters of PSCs based on different perovskite materials, MAPbI₃, FAPbI₃, MAFAPI₃ and CsMAFAPI₃, are discussed in the second section.

Besides, CIGS, with a tailorable direct band gap (of 1.04–1.68 eV), can serve as bottom cell with excellent band gap match with perovskites (1.6–2.3 eV) [19] in the combined monolithic perovskite/CIGS tandem solar cell. This flexible tandem solar cell device promises high PCE that exceeds the Shockley–Queisser limit, enabling cost-efficient and ultra-lightweight cells for applications in terrestrial and space photovoltaics with power-to-weight and power-to-cost ratios surpassing individual cells and those of III-V semiconductor-based multijunctions [20]. Thus, it is important to realize the compositional and thermal stability among different substrates and perovskite materials. Furthermore, the degradation behavior of PV parameters with thermal stability is studied in detail for commercially available perovskite and CIGS solar cells. Such studies will help to investigate the degradation processes that have been mainly responsible for reduction in PV parameter performance. Here, we investigate the performance characteristics as function of temperatures, higher or lower than STC, for the understanding and prediction of solar cell performance in real-world working conditions, from applications point of view as well as in manufacturing.

2 CIGS solar cells: photovoltaic parameters as a function of substrate material and influence of substrate temperature

CIGS solar cells have demonstrated good performance for most of the visible spectrum under terrestrial conditions at high operating temperature (350 K); besides, they can also be used for space applications due to their high radiation tolerance [21]. Generally, for most semiconductors, E_g decreases with increase in temperature. Therefore, increasing temperature contributes to the increase in J_{sc} and decrease in V_{oc} ; besides, the increasing temperature,

in general, increases the probabilities of recombination which eventually leads to the reduction in PCE [22]. The temperature dependence of efficiency of CIGS solar cells is of great relevance, such as for space applications in which panels are subjected to temperatures varying from 80 to 380 K within a few minutes after eclipse [18] and also for terrestrial applications where they could be subjected to environmental temperatures as high as 350 K. The PV parameters of CIGS solar cells on three different types of substrates, SLG (Sodium Lime Glass), SS (Stainless Steel foils) and PI (Polyimide), are studied in order to assess the influence of the substrate on the internal operation of the cell.

2.1 Effect of different substrates on photovoltaic parameters

The substrates in CIGS solar cells have a crucial role in the development of the whole device. Deposition of the Mo back contact on SLG or flexible substrate will define different selenization conditions [23]. Conventionally, most commercial CIGS solar cells are produced on SLG substrates since SLG provides a sufficient source of Na (alkali metal) to the absorber naturally [24] and is able to sustain high temperature during deposition and annealing processes. In recent years, CIGS solar cells deposited on light weight and flexible substrates have been studied for versatile applications [25]; for example, flexible CIGS solar cells can be integrated on rooftops or as a bending module with curved surface. So far, efficiencies of 22.8% on SLG substrate [8], 17.5% on SS substrate [26] and 20.4% PI substrate [27] for CIGS solar cells have been achieved. Among various SS substrates, stainless Cr steel is expensive but with lower coefficient of thermal expansion, and unalloyed Fe steel is cheaper but with the corrosion issue and higher coefficient of thermal expansion (13 ppm K⁻¹ for Cr-free steel compared to 11 ppm K⁻¹ for Cr steel at 823 K) [28]. Besides SS substrates, PI substrate is an attractive choice due to its vacuum and temperature stability and is considered as a good candidate for alkali doping technology; it can be readily accomplished due to the fact that only a small amount of impurities diffuse out of the PI substrate [29].

In Fig. 2, the data on the V_{oc} - T relationship of CIGS solar cells on SS, PI and SLG substrates, from the recent 10 years of literature, are summarized. The results show a consistent and negatively linear behavior with high correlation factor ($R^2 > 0.998$), for a variety of substrates, which eventually can be attributed to a reduction in the PCE for the temperature range of 100–360 K. Besides, V_{oc} on SLG substrate has continuously higher value than alkali-doped PI substrate and SS substrate, which may be due to the presence of lower concentration of

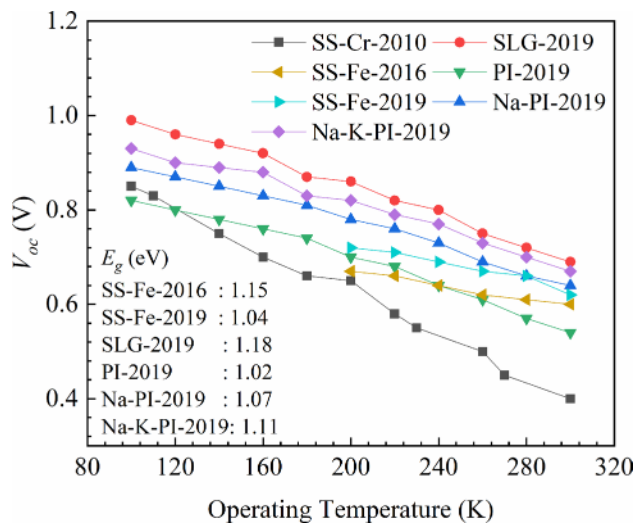


Fig. 2 V_{oc} - T plot for different substrates. The data in the figure are extracted from Refs. [29–32]

defects or better absorber quality on SLG substrate. CIGS solar cells on alkali-doped PI substrates, Na-PI-2019 and Na-K-PI-2019, performed better than undoped PI and SS substrates. Especially, the performance of CIGS solar cells on Na-K-PI-2019 is very close to that of CIGS solar cells on SLG-2019; the difference in V_{oc} values may be attributed to the differences within CIGS and may not be due to the substrate. This confirms that in addition to Na content, the incorporation of K from the substrate into CIGS helps to passivate the defects via inter-diffusion of In and Ga atoms and suppress the recombination process in the CIGS absorber [29]. The diffusion of the detrimental impurities (e.g., Fe) increases with increasing temperature and is a major challenge for high-efficiency CIGS modules on SS substrates, in which barrier layers are normally used to prevent this impurity diffusion [33, 34]. E_g of CIGS can be varied from 1.04 to 1.68 eV by varying the composition within CIGS to absorb most of the photons. In Fig. 2, we also notice that the change in V_{oc} , as function of V_{oc} - T , is almost uniform and is generally independent of E_g . Further, in Fig. 2, the CIGS films on similar SS-Fe substrates (SS-Fe-2016, $E_g = 1.15$ [35]; SS-Fe-2019, $E_g = 1.04$ [36]) showed that the CIGS films with higher E_g exhibited better thermal stability than CIGS films with lower E_g . This is the same case with CIGS films on PI substrates with and without alkaline doping to advance the material properties and E_g .

From two simulation studies, shown in Fig. 3, it can be noted that J_{sc} decreases slightly with increasing temperature in the temperature range of 260–370 K. This slight decrease in J_{sc} is ascribed to reflection losses (series and shunt resistance) and recombination losses, as described by Eq. (2). [4]. However, CIGS on PI substrate showed a

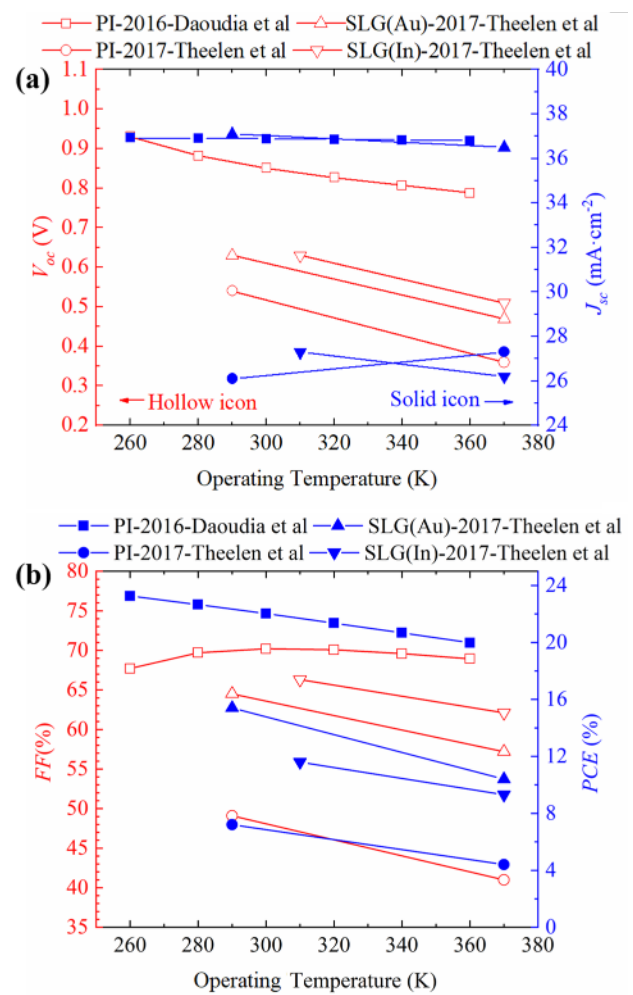


Fig. 3 Temperature dependence of PV parameters (e.g., PCE, FF, V_{oc} and J_{sc}). The structure of CIGS solar cell [2016-Daoudia et al.-PI] is PI/Mo/CIGS/CdS/i-ZnO/ZnO:B; for (2017-Theelen et al.-PI) is PI/Mo/CIGS/CdS/i-ZnO/ZnO:Al; for (2017-Theelen et al.- (SLG(Au)) is SLG/Mo/CIGS/CdS/i-ZnO/ZnO:Al/Au). The data in figure are extracted and regenerated from Refs. [37, 38]

slightly positive temperature dependence on J_{sc} , which is different from the others.

$$J_{sc} = q \int_{hv=E_g}^{\infty} \frac{dN_{ph}}{dh\nu} d(h\nu) \quad (2)$$

As a consequence, most of the PV parameters (e.g., FF, V_{oc} and J_{sc}) have similar trends in temperature dependency on different substrates, mostly, a negative trend. In accordance with Eqs. (3)–(5), we can conclude that PCE decreases with increasing temperature as temperature has a positive impact on the intrinsic carrier concentration (n_i). J_o increases with increasing n_i which further decreases the V_{oc} . The steady loss of J_{sc} on SLG substrate

or slight increase on PI substrate, in which the J_{sc} is not enough to compensate for the loss of V_{oc} , eventually lead to decreased FF and PCE with increasing temperature. J_o , saturation current density, is proportional to the square of the intrinsic carrier concentration for a solar cell which has been modeled [39] as in Eq. (3).

$$J_o = q \times B \times \left(\frac{D_n}{L_n N_A} + \frac{D_p}{L_p N_D} \right) n_i^2 \quad (3)$$

where q is the electronic charge, n_i is the intrinsic carrier density, B is another constant independent of temperature, N_A and N_D are densities of acceptor and donor atoms, D_n and D_p are diffusion constants of minority carriers in p and n regions, and L_n and L_p are length of minority carriers in p and n regions, respectively. As seen from Eq. (3), J_o is strongly determined by the proportionality to $\sim n_i^2$ and n_i can be represented as in Eq. (4).

$$n_i^2 = A \times T^3 \times \exp\left(-\frac{E_g}{kT}\right) \quad (4)$$

By combining Eqs. (3) and (4), in the presumption of temperature dependence of all parameters except n_i , the expression for J_o can be written in terms of temperature and bandgap energy [40] as in Eq. (5), where C is the third constant independent of temperature.

$$J_o = C \times T^3 \times \exp\left(-\frac{E_g}{kT}\right) \quad (5)$$

Moreover, a deduction is made that SS substrate should hold the same temperature dependency on PV parameters as PI and SLG. Besides, it should be noted that the obvious difference in the values between the same substrates from two literatures may be due to the large variation between individual CIGS solar cells. But the temperature dependence of PV parameters of CIGS, when deposited on different substrates (e.g., SLG, SS and PI), has mostly the same relationship.

2.2 Effect of substrate temperature on electrical properties

High substrate temperature will not only enhance the growth of the absorber layer but also favor alkali-diffusion from substrate to absorbers. Most of the high-efficiency CIGS modules have been prepared at substrate temperature (T_{sub}) of over 773 K which is very close to the softening temperature of SLG substrates [41]. Low substrate temperature (< 723 K) provides the feasibility for reducing the thermally induced stress on the substrate, for example, by depositing Mo on PI [42]. PI substrate is suitable for continuous and rapid roll-to-roll deposition process and hence

reduces the manufacturing cost of CIGS solar cell module [43]. The use of PI substrate reduces the T_{sub} and can lead to a decrease in manufacturing costs. The use of high substrate temperature with glass substrates promises enough thermal energy to form high-quality CIGS films. T_{sub} also plays an important role in providing the thermal energy for the inter-diffusion between atoms, which is also related to the phase transformations in the growth process of CIGS. Here, we investigate the effect of T_{sub} on the structural and electrical properties of CIGS films on various substrates.

In the case CIGS/SLG, with T_{sub} in the temperature range of 623–773 K, by using one-stage co-evaporation process [44], the enhancement in PCE, FF and V_{oc} is observed when T_{sub} is increased from 573 to 773 K. Especially, a significant increase, above a critical temperature of 723 K, is observed due to the drastic increase in carrier concentration. This is because of the diffusion of Na content from SLG into the CIGS absorber at temperatures above 723 K, which also decreases the resistivity. The FF and V_{oc} have similar increasing trends as PCE which may be ascribed to the improvement in Na diffusion at higher temperature on SLG substrates [45]. Additionally, the decrease in V_{oc} with decreasing T_{sub} can be explained by recombination occurring in the grain boundary due to the smaller grain size at low temperature [46]. Low J_{sc} values at lower temperature (< 673 K) can be attributed to the poor quality of CIGS films which reduces the carrier collection. It is worthwhile to note that many papers in the literature have reported slight decrease in J_{sc} after the substrate temperature reaches ~ 823 K, which is in contrast to other parameters such as FF, V_{oc} and PCE [44, 47]. Similar results of PV parameters with T_{sub} can be observed in the literature [44, 47, 48], for the case of CIGS cells/SLG substrates which have the same structure of glass/Mo/CIGS/CdS/i-ZnO/Al-ZnO. It is commonly expected that, with increase in T_{sub} (over 800 K), the enhancement of larger grain growth occurs. Eventually, they form big blocks of grains when T_{sub} is in the temperature range of 823–873 K, which shows that high T_{sub} can give enough thermal energy to form high-quality CIGS films. The high PCE at T_{sub} of 823 K is related to Na incorporation and the disappearance of secondary-phase $(\text{In}_{0.62}\text{Ga}_{0.38})_2\text{Se}_3$, which helps to process films with better structural properties.

In 2016, Liang et al. [31] studied the influence of T_{sub} on CIGS module (SS/Mo/CIGS/CdS/i-ZnO/n-ITO/Al) with the cells deposited on SS substrate using a 3-stage co-evaporation process. In this case, V_{oc} increases with increasing substrate temperature but reaches a slow trend for T_{sub} above 783 K. This may be due to a wider E_g that can be achieved with a higher T_{sub} , which can effectively decrease the saturation current and therefore increase the V_{oc} [49]. The comparison of $V_{oc}-T$ and $J_{sc}-T$ behavior of Liang's study on SS substrate with other studies in the literature

on different substrates (e.g., SLG and PI) is presented in Fig. 4a. It may be noted that J_{sc} initially increases and then decreases with temperature > 773 K, which is also observed in the $J_{sc}-T$ relationship on SLG substrate. Here, the author suggests that the decrease in J_{sc} as the substrate temperature ~ 773 K may be ascribed to the increasing Fe concentration, which could replace In and Ga lattice sites and enhance the recombination probabilities [28]. The comparison of FF– T and PCE– T behavior between Liang’s study on SS substrate and other studies in the literature on different substrate (e.g., SLG and PI) can be seen in Fig. 4b. In addition, low FF values for lower substrate temperature (< 723 K) for both SS and SLG substrates can be ascribed to the larger grain boundaries. However, for high substrate temperature, close enough to material

softening temperature (in the case of SS substrate, it is ~ 773 K), impurities of high concentration may diffuse into CIGS modules and act as shunt path [33]. The same relationship between PV parameters and T_{sub} is observed in the literature, for example, Zortea et al. [32] on unalloyed SS substrate by using a 3-stage co-evaporation process. In recent years, the use of SS substrate has caught researchers’ interests due to a better substrate temperature dependence of PV parameters with polished surfaces (low irregularities), which could possibly reduce pin holes and shunts during subsequent processing [30]. In the study reported by Zortea et al. [32], impurity concentration increases with increasing substrate temperature which causes defect states and leads to additional recombination losses, as shown in Fig. 5. This eventually leads

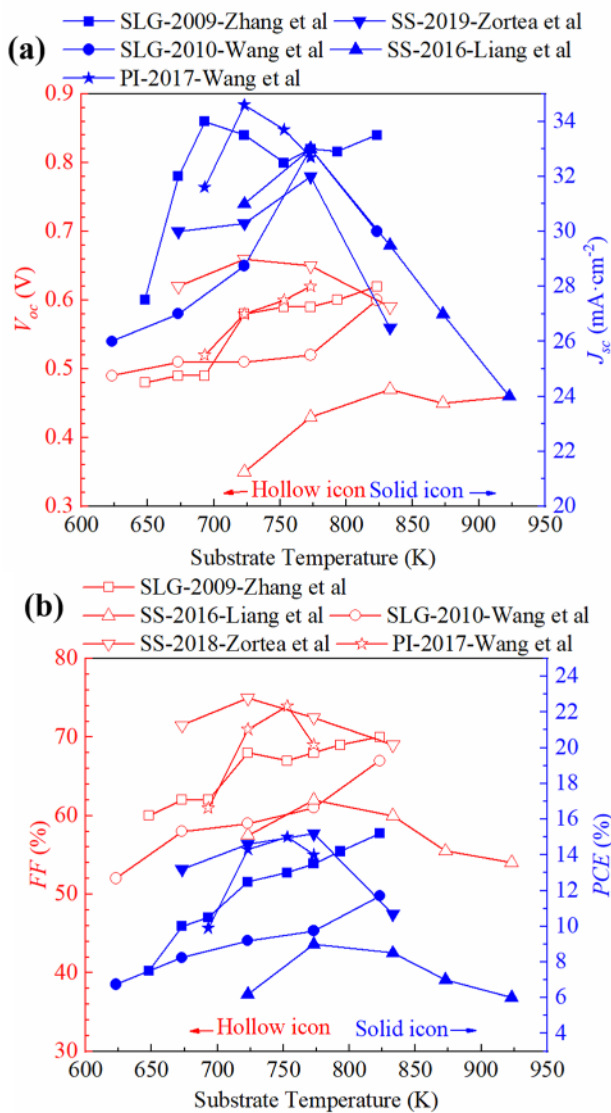


Fig. 4 J - V parameters of CIGS solar cells on different substrates at different T_{sub} . Data extracted from Ref. [31, 32, 44, 45, 50]

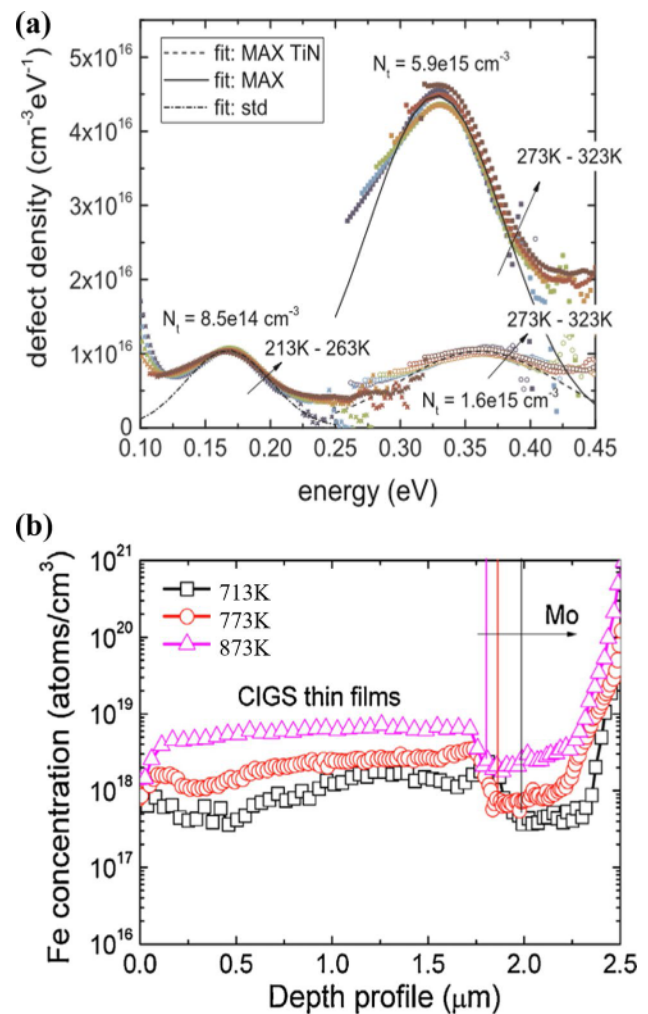


Fig. 5 **a** Calculated defect spectra of solar cell on SS substrate of MAX (T_{sub} of 833 K), std (T_{sub} of 723 K) and Max TiN (SS substrate with TiN barrier layer at T_{sub} of 833 K) **b** Fe content profiles in CIGS solar cell on SS substrate for T_{sub} of 713 K, 773 and 873 K by SIMS measurements. Reprinted and reproduced with permission from Ref. [31] and Ref. [32], respectively

to a decrease in efficiency for high T_{sub} (> 773 K). Thus, a more precise control of the processing temperature would facilitate in designing a distinct T_{sub} profile for growing CIGS on SS substrates. The diffusion barrier layer between the substrate and the Mo back contact is also helpful to suppress the diffusion of detrimental elements from the substrate into the CIGS when T_{sub} is < 773 K.

It is well known that CIGS absorbers in high-efficiency cells are normally deposited at high T_{sub} (> 823 K) on rigid SLG substrates. However, for temperature sensitive flexible PI substrates, its thermal stability limits the process temperatures to about 723 K, which is 100 K less than SLG; thus, a low substrate temperature deposition technique is necessary while deploying flexible substrates. Zhang et al. [50] investigated the PV properties of CIGS solar cell (Mo/CIGS/CdS/i-ZnO/n-ZnO:Al/Al grid) on SLG and PI substrate in the temperature range of 673–773 K, by using a 3-stage co-evaporation process. The results show that V_{oc} increases with increasing substrate temperature (T_{sub} in the range of 673–753 K) and decreases for $T_{\text{sub}} > 753$ K. FF of CIGS cells on PI substrate increases with increasing T_{sub} ; the lower FF of CIGS cells on PI substrates than those on SLG may be ascribed to the large grain boundaries [51] and the shunt resistance caused by the relatively rough surface of PI substrate. This reasoning is also consistent with studies of CIGS cells on SS substrate as reported by Zortea et al. [32]. It should be noted that the CIGS solar cell on PI substrate exhibits higher J_{sc} values due to the higher spectral response in the long wavelength range of 550–1100 nm [50]. T_{sub} has a stronger influence on PI with respect to the thermal absorption and emission properties when compared with SLG [50]. Accordingly, the CIGS absorber with relatively low defects, formed on PI, leads to a relatively long carrier lifetime and a reduction in recombination probabilities.

3 Perovskite solar cell photovoltaic parameters as function of material properties and influence of temperature

Hybrid organometal halide perovskite materials, such as MAPbI_3 , FAPbI_3 and $\text{MA}_x\text{FA}_{(1-x)}\text{PbI}_3$ have been investigated widely for light harvesting in PSCs. In most recent studies, PSCs based on: (a). MAPbI_3 have achieved 21% PCE [35]; (b). FAPbI_3 have achieved 21.07% PCE [36] and (c). $\text{MA}_x\text{FA}_{(1-x)}\text{PbI}_3$ have achieved 21.6% PCE [52, 53]. Inorganic Cs ion has been used to enhance the thermal stability of perovskite cation combinations (e.g., Cs/MA, Cs/FA, and Cs/MA/FA); this has resulted in cells with 20.32% PCE. [54, 55] Commonly, PCE is measured in the laboratory under standard test conditions (STCs, 25 °C and AM1.5G with 100mWcm^{-2}). However, solar cells in the working

condition will operate at lower and higher temperatures, leading to changes (and often a decrease) in the average PCE, as reported for silicon solar cells [56]. Apart from the importance of material characteristics affecting the performance of PSCs, temperature-dependent photovoltaic behavior of PSCs is also highly desirable to study. $\text{Cs}_{0.05}(\text{MA}_{0.17}\text{FA}_{0.83})_{0.95}\text{Pb}(\text{I}_{0.83}\text{Br}_{0.17})_3$, with $E_g = 1.62$ eV [20], has been investigated and has been shown to exhibit high thermal stability for applications in PSCs.

3.1 Hybrid organometal halide perovskites: MAPbI_3 , FAPbI_3 , MAFAPbI_3 and CsMAFAPbI_3 -based solar cells

As stated by Shockley and Queisser, in general, the E_g of the semiconductor affects the performance of the cell [57]. Seok et al. showed that the E_g of perovskites can be changed by altering the length of lead and halide site, by either changing the halide, the metal or the ion size [58]. Particularly, the E_g of the perovskite decreases when changing the cation from MA to larger FA cation [59]. In this work, an analysis of the PV parameters of PSCs, at operating temperatures in the range of 80–360 K, based on different perovskite materials, such as MAPbI_3 ($\text{CH}_3\text{NH}_3\text{PbI}_3$), FAPbI_3 (NH_2CHNH_2), $\text{MA}_x\text{FA}_{(1-x)}\text{PbI}_3$ and CsMAFAPbI_3 , is presented. The temperature activated formation and migration of ionic defects within the perovskite lattice remains a potential source of instability for perovskite photovoltaics [60, 61]. In Table 1, a summary of the dependence of E_g and J_{sc} on operating temperature for FTO/TiO₂/TiO₂/MAPbI₃/Spiro-OMeTAD/Au is presented (Extracted from results

Table 1 Dependence of E_g and J_{sc} on operating temperature for FTO/TiO₂/TiO₂/MAPbI₃/Spiro-OMeTAD/Au. Extracted from results based on Ref. [62]

Temperature K	E_g eV	J_{sc} $\text{mA}\cdot\text{cm}^{-2}$
100	1.567	15.8
120	1.566	15.6
140	1.566	15.1
160	1.570	15.8
180	1.571	15.9
200	1.575	16.1
220	1.576	16.2
240	1.576	16.5
260	1.579	16.7
280	1.581	16.8
300	1.585	16.5
320	1.587	16.6
340	1.586	17.2
360	1.592	16.2

based on Ref. [62]). As can be seen in Table 1, with increase in operating temperature, the energy gap increases; J_{sc} decreases initially and subsequently increases.

In Fig. 6a, b, we investigate the properties of perovskite solar cells based on MAPbI₃, from two sources of literature. In the first reference (2015-Zhang), for mesoscopic PSCs (TiO₂/MAPbI₃/Al₂O₃/NiO/carbon) [64], V_{oc} follows a volcano-like distribution with the maximum value at ~260 K under constant light intensity and decreases at operating temperatures in the range of ~220–260 K. This decrease is ascribed to charge accumulation near perovskite/electrode interface; the unit cell equilibrium and polarizability are very sensitive to temperature. Normally, V_{oc} of PSCs have higher value than other candidate cells (e.g., CIGS solar cell and silicon heterojunction solar cell); this is due to the larger E_g (> 1.4 eV) of the perovskites. Furthermore, it has been reported that V_{oc} decreases with decreasing light intensity (from 1 sun to 0.1 sun), which indicates that the permittivity of perovskites plays a critical role in the V_{oc} - T behavior [64]. J_{sc} increases with increasing

temperature, reaching the maximum value (~22 mA cm⁻²) at around 240 K, which is almost the same for a different PSC structure (FTO/compact TiO₂/porous TiO₂/MAPbI₃/Spiro-OMeTAD/Au) [63]. In Fig. 6a, J_{sc} (for 2017-Wang) has higher value at low temperature (80–200 K) and higher maximum value (~23 mA cm⁻²) (than 2015-Zhang), which may be due to the better transportation ability of photo-generated holes within the perovskite/NiO interface and electrons within the percolated perovskite/TiO₂ networks [64]. In Fig. 6b, the low FF at low temperature (< 250 K) is due to the increased charge carrier diffusion resistance in the MAPbI₃ layer. FF increases significantly when the temperature is > 240 K and its maximum value is attained at 300 K. This increase compensates for the unavoidable decrease in V_{oc} at elevated temperature (normally, > 260 K) (Fig. 6a). As a consequence, PCE increases with increasing temperature (Fig. 6b) and attains a maximum value at 280 K. A decrease in PCE for low temperature (bottom red curve in Fig. 6b) and higher temperature (> 300 K in Fig. 6b) may be due to temperature-activated charge transport in

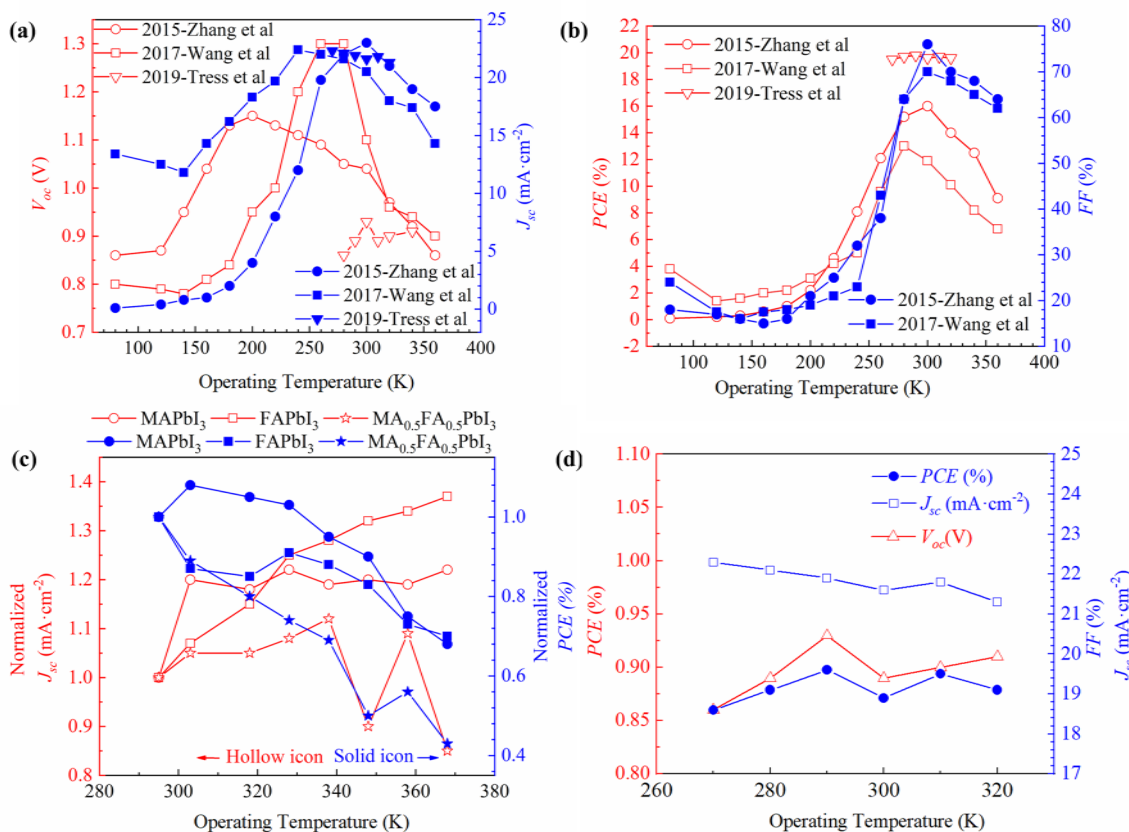


Fig. 6 Temperature dependence of **a** PCE and FF and **b** V_{oc} and J_{sc} of MAPbI₃-based PSCs extracted from literature, 2015-Zhang et al., on PSC (FTO/compact TiO₂/porous TiO₂/MAPbI₃/Spiro-OMeTAD/Au); and 2017-Wang et al., on PSCs (TiO₂/MAPbI₃/Al₂O₃/NiO/carbon) and 2019-Tress et al., on CsMAFAPbI_xBr_(1-x)-based PSC. **c** Com-

parison of normalized J_{sc} -PCE- T of PSCs based on various perovskite materials. **b**, **c** Comparison of temperature dependence of PV parameters of MAPbI₃, FAPbI₃, MAFAPI₃ and CsMAFAPbI_xBr_(1-x) ($X=0-1$); **a**, **b** are extracted from 2015-Zhang (Ref. [63]) and 2017-Wang (Ref. [64]) **c** extracted from Ref. [65]

charge transport layers (in particular, spiro-OMe-TAD [66]) affecting series resistance and FF, which is similar to other works in the literature [64, 67].

The temperature dependence of PV parameters of PSCs (FTO/TiO₂ compact layer/Mesoporous TiO₂/Perovskite/Au), based on three perovskite materials, MAPbI₃, FAPbI₃ and MAFAPbI₃, is presented in Fig. 6c (based on data extracted from Ref. [65]). FAPbI₃ has an E_g of 1.46 eV which is lower than that of MAPbI₃ (E_g of 1.57 eV) and MAFAPbI₃ (E_g of 1.53 eV). The absorption edge, λ_e ($= 1240/E_g$; E_g in eV), of FAPbI₃ is 850 nm, showing better performance than MAPbI₃ (790 nm) as a light harvester. The increasing temperature will generally decrease the E_g of a semiconductor material which will eventually lead to a decrease in PCE. The result in Fig. 6c shows that J_{sc} increases by ~30% which may be due to the better stability of FAPbI₃ at high temperature (> 340 K). However, this increase is not enough for the compensation of the loss of FF and V_{oc} values, which eventually results in a low PCE. An interesting phenomenon is that MAFAPbI₃ shows severe degradation of the PV parameters with increasing temperature. This may be due to the formation of different strain inside the crystalline structure for both MAPbI₃ and FAPbI₃ due to increasing temperature [65]. The decrease in V_{oc} with increasing temperature, due to the higher recombination probabilities, results in a decrease in PCE. Besides, the intrinsic carrier concentration depends on E_g . The main reason for the decrease in PCE at temperatures > 280 K is due to the photocurrent hysteresis effect that exists in most of the PSC devices, which has been described in detail in the literature [68]. Although MAPbI₃, FAPbI₃ and MAFAPbI₃ perovskite solar cells have exhibited high efficiencies, their long-term stability is still a concern for PSCs to be commercialized. The thermal degradation temperature (phase transition temperature) of perovskite materials in PSC are ~328–358 K for MAPbI₃ and > 373 K for FAPbI₃ [69]. The implication is that these perovskite materials have thermal stability problems in working conditions (273–353 K).

Recent studies have shown that, with the addition of inorganic cations (e.g., Cs and/or Rb), the compositions of perovskites can be thermally stable at temperatures > 373 K [70]. CsMAFAPbI_xBr_(1-x) ($X = 0-1$)-based perovskite solar cell has a wide tunable band gap from 1.4 to 2.3 eV and improved light and moisture stability compared with FAPbI₃, which enhances its PCE [71]. Thus, it becomes a matter of design while using hybrid perovskite materials in which the perovskite is combined with various cations and halides. In 2019, Tress et al. [67] investigated the temperature dependence (273–323 K) of PV parameters with the conditions that were acquired from real-world weather records (Lausanne, Switzerland) and compared their results with silicon heterojunction

(SHJ) cell. In this study, the structure of the PSC is FTO/perovskite/TiO₂/Spiro-MeOTAD/Au with CsFAPb(I_{0.83}Br_{0.17})₃ perovskite. The authors reported a monotonous increase in V_{oc} from ~0.85 to 0.95 and then decrease to 0.9 V with increasing temperature, which is similar to the behavior of cells of other perovskite materials (e.g., MAPbI₃, FAPbI₃ and MAFAPbI₃) in the same temperature range, as shown in Fig. 6d. Besides, the change (increasing and decreasing pattern) in PCE can be considered to be almost negligible with slight increase or decrease from 19.5 to 19.8% and then to 19.6%. Accordingly, we assume that PSCs are less affected by temperature in the range of 300–323 K because of the advantages obtained by adding Cs ion into MAFAPbI_xBr_(1-x) ($X = 0-1$) which effectively avoids the light soaking problem and reduces the recombination traps [72]. Conventional MAPbI₃ and FAPbI₃ perovskites can be improved by the addition of multiple cations; the different size of the cations compensates the MAPbI₃-type perovskites to lead to new multi-cation perovskites that have several advantages. It has been shown that RbCsMAFAPbI₃ PSCs exhibit low degradation (5%) in PCE after subjecting the device at 85 °C under continuous illumination (500 h) with full intensity at maximum power point (MPP) [52]. As a consequence, with the addition of inorganic cation (e.g., Cs and Rb) into MAFAPbI₃ perovskite, the suppression of halide segregation and wide and tunable band gaps that are beneficial and suitable not only for perovskite solar cells, but also with significant compositional properties for tandem solar cells (e.g., perovskite/CIGS and perovskite/silicon) has been demonstrated [52].

Most of the investigations of the temperature dependence of PV parameters in PSCs focus on perovskites based on single cation (MAPbI₃ or FAPbI₃) and double cation (MAFAPbI₃), which show a relative stable performance around room temperature with a significant decrease in performance at both high and low temperatures. Marko Jost et al. [73] report a low-power temperature coefficient of $-0.17\% \text{ K}^{-1}$ under the outdoor condition testing, which also shows that perovskite solar cells (FAMAPbI₃) are highly thermally stable under increasing temperature at a range between 25 and 85 °C. In addition to temperature-dependent measurements, the aging test of temperature cycle for the module has been studied recently. In the study by Checharoen et al. [74], almost no degradation of PCE has been observed when the solar cells are encapsulated and cycled between 243 and 358 K in dark experimental conditions. Domanski et al. [75] have shown that CsMAFAPbI₃-based PSC exhibits lower degradation rate during the temperature cycle (from 263 to 338 K). In this experiment, the PSC module was stressed with the device held continuously at 338 K; degradation was observed in the Hole Transport Material (HTM). Furthermore, Jonas A. Schwenzler et al. [76] compared the

degradation of PCE and other PV parameters between MAPbI₃, MAFApI₃ and triple cation (CsMAFApI₃). The results show that CsMAFApI₃ has low degradation and maintains high PCE for long running time with a cycling temperature test (from room temperature to high temperature of 333 K and then back to room temperature). Cs_{0.05}(MA_{0.17}FA_{0.83})_{0.95}Pb(I_{0.83}Br_{0.17})₃, with $E_g = 1.62$ eV [20], has been demonstrated as one of the perovskite materials with high thermal stability for the fabrication of PSCs. Moreover, by combining this perovskite as the top solar cell with CIGS solar cell processed on flexible substrate as the bottom solar cell, PCE of 25% has been shown for the solar cell module [77].

4 Conclusion

The temperature dependence of PV parameters of CIGS and perovskite solar cells is investigated, as function of operating temperature and substrate temperature. T_{sub} at 823 K is critical for CIGS on SLG substrates, where Na incorporates into the CIGS absorber and lowers the resistivity. SS substrates can sustain T_{sub} as high as SLG substrate; however, the diffusion of the detrimental impurities (e.g., Fe) increases with increasing temperature; this is a major challenge for high PCE CIGS modules on Fe containing SS substrates. Increased grain boundary density and defects contribute to large resistivity when T_{sub} is low.

In general, the PCE of PSC showed slight temperature dependence, in contrast to CIGS solar cells. The operating temperature dependency of both perovskite and CIGS solar cells is initially due to the effect of V_{oc} on temperature. The variation in V_{oc} is mainly from the defect concentration which can be attributed to high recombination rate with increasing temperature. For most perovskite solar cells, J_{sc} in general, increases with increasing temperature from lower temperature to around ~ 250–280 K. For future development, this work provides useful information for the design and understanding of stable, high-efficiency thin-film solar cells which have the potential for working in terrestrial and space applications.

The comparison of substrate temperature and operating temperature, based on different substrates of CIGS solar cells, provides the knowledge of advantages and disadvantages that are associated with using each substrate material. The development of perovskite material has the trend to couple the alkaline cations (e.g., Cs and Rb) to improve the thermal stability. The side-by-side discussion provides the insight into which composition of the perovskite material has the most thermal tolerance with better PV performance parameters and the effect of temperature on different substrates for CIGS solar cells. This study is useful to determine/identify the best possible

combination of perovskite/CIGS tandem solar cell that has high PCE for real-world working conditions. Besides, in real-world applications, the thermal testing procedures are critical for assessing the life expectancy of the device; thus, this temperature dependence study provides results for each perovskite and CIGS solar cell on different substrates.

Author contributions Equal.

Data availability Not applicable.

Compliance with ethical standards

Conflicts of interest The authors declare no conflicts of interest.

Code availability Not applicable.

Ethical approval Not applicable.

References

1. Fraunhofer Institute for Solar Energy Systems. PHOTOVOLTAICS REPORT. Fraunhofer www.ise.fraunhofer.de. Accessed 17 June 2020
2. Theelen M, Daume F (2016) Stability of Cu (In, Ga) Se₂ solar cells: a literature review. *Solar Energy* 133:586–627. <https://doi.org/10.1016/j.solener.2016.04.010>
3. Lee TD, Ebong AU (2017) A review of thin film solar cell technologies and challenges. *Renew Sustain Energy Rev* 70:1286–1297. <https://doi.org/10.1016/j.rser.2016.12.028>
4. Singh P, Ravindra NM (2012) Temperature dependence of solar cell performance—an analysis. *Solar Energy Mater Solar Cells* 101:36–45. <https://doi.org/10.1016/j.solmat.2012.02.019>
5. Wysocki JJ, Rappaport P (1960) Effect of temperature on photovoltaic solar energy conversion. *J Appl Phys* 31(3):571–578. <https://doi.org/10.1063/1.1735630>
6. Varshni YP (1967) Temperature dependence of the energy gap in semiconductors. *Physica* 34(1):149–154. [https://doi.org/10.1016/0031-8914\(67\)90062-6](https://doi.org/10.1016/0031-8914(67)90062-6)
7. Devaney WE, Mickelsen RA (1988) Vacuum deposition processes for CuInSe₂ and CuInGaSe₂ based solar cells. *Solar Cells* 24(1):19–26. [https://doi.org/10.1016/0379-6787\(88\)90032-4](https://doi.org/10.1016/0379-6787(88)90032-4)
8. Kato T, Wu JL, Hirai Y, Sugimoto H, Bermudez V (2018) Record Efficiency for thin-film polycrystalline solar cells up to 22.9% achieved by Cs-Treated Cu(In,Ga)(Se,S)₂. *IEEE J Photovolt* 9(1):325–330. <https://doi.org/10.1109/JPHOTOV.2018.2882206>
9. Ball JM, Lee MM, Hey A, Snaith HJ (2013) Low-temperature processed meso-superstructured to thin-film perovskite solar cells. *Energy Environ Sci* 6(6):1739–1743. <https://doi.org/10.1039/c3ee40810h>
10. Green M, Ho-Baillie A, Snaith H (2014) The emergence of perovskite solar cells. *Nat Photonics* 8:15–20. <https://doi.org/10.1038/NPHOTON.2014.134>
11. Kojima A, Teshima K, Shirai Y, Miyasaka T (2009) Organometal halide perovskites as visible-light sensitizers for photovoltaic cells. *J Am Chem Soc* 131(17):6050–6051. <https://doi.org/10.1021/ja809598r>
12. Yang WS et al (2017) Iodide management in formamidinium-lead-halide-based perovskite layers for efficient solar cells.

- Science 356(6345):1376–1379. <https://doi.org/10.1126/science.aan2301>
13. Jošt M et al (2019) 21.6%-efficient monolithic perovskite/Cu(In,Ga)Se₂ tandem solar cells with thin conformal hole transport layers for integration on rough bottom cell surfaces. *ACS Energy Lett* 4(2):583–590. <https://doi.org/10.1021/acsenerylett.9b00135>
 14. Brenner TM, Egger DA, Kronik L, Hodes G, Cahen D (2016) Hybrid organic—inorganic perovskites: low-cost semiconductors with intriguing charge-transport properties. *Nat Rev Mater* 1(1):15007. <https://doi.org/10.1038/natrevmats.2015.7>
 15. Palmstrom AF et al (2019) Enabling flexible all-perovskite tandem solar cells. *Joule* 3(9):2193–2204. <https://doi.org/10.1016/j.joule.2019.05.009>
 16. Carron R et al (2018) Refractive indices of layers and optical simulations of Cu(In, Ga)Se₂ solar cells. *Sci Technol Adv Mater* 19(1):396–410. <https://doi.org/10.1080/14686996.2018.1458579>
 17. Singh P, Singh SN, Lal M, Husain M (2008) Temperature dependence of I–V characteristics and performance parameters of silicon solar cell. *Solar Energy Mater Solar Cells* 92(12):1611–1616. <https://doi.org/10.1016/j.solmat.2008.07.010>
 18. Liu S, Simburger E, Matsumoto J, Garcia A, Ross J, Nocerino J (2005) Evaluation of thin-film solar cell temperature coefficients for space applications. *Prog Photovolt Res Appl* 13:149–156. <https://doi.org/10.1002/pip.602>
 19. Leijtens T, Bush KA, Prasanna R, McGehee MD (2018) Opportunities and challenges for tandem solar cells using metal halide perovskite semiconductors. *Nat Energy* 3(10):828–838. <https://doi.org/10.1038/s41560-018-0190-4>
 20. Lang F et al (2020) Proton radiation hardness of perovskite tandem photovoltaics. *Joule* 4(5):1054–1069. <https://doi.org/10.1016/j.joule.2020.03.006>
 21. Ramanujam J, Singh UP (2017) Copper indium gallium selenide based solar cells—a review. *Energy Environ Sci* 10(6):1306–1319. <https://doi.org/10.1039/c7ee00826k>
 22. Fan JCC (1986) Theoretical temperature dependence of solar cell parameters. *Solar Cells* 17(2):309–315. [https://doi.org/10.1016/0379-6787\(86\)90020-7](https://doi.org/10.1016/0379-6787(86)90020-7)
 23. Ong KH et al (2018) Review on substrate and molybdenum back contact in CIGS thin film solar cell. *Int J Photoenergy* 2018:9106269. <https://doi.org/10.1155/2018/9106269>
 24. Li W, Yan X, Aberle AG, Venkataraj S (2017) Effect of a TiN alkali diffusion barrier layer on the physical properties of Mo back electrodes for CIGS solar cell applications. *Curr Appl Phys* 17(12):1747–1753. <https://doi.org/10.1016/j.cap.2017.08.021>
 25. Marlein J, Khelifi S, Burgelman M, Belghachi A (2008) Electrical characteristics of Cu(In,Ga)Se₂ thin films solar cells on metallic foil substrates. *Mater Sci* 10:15–20. <https://doi.org/10.4229/23rdeupvsec2008-3do.5.6>
 26. Szalaj A, Keane J, Tuttle JR (2000) Conference record of the 28th IEEE photovoltaic specialists conference. Anchorage, AK, USA., Sept 2000, p 1042
 27. Chirilă A et al (2013) Potassium-induced surface modification of Cu (In, Ga) Se₂ thin films for high-efficiency solar cells. *Nat Mater* 12(12):1107–1111. <https://doi.org/10.1038/nmat3789>
 28. Wuerz R et al (2009) CIGS thin-film solar cells on steel substrates. *Thin Solid Films* 517(7):2415–2418. <https://doi.org/10.1016/j.tsf.2008.11.016>
 29. Kim K et al (2020) Mechanisms of extrinsic alkali incorporation in CIGS solar cells on flexible polyimide elucidated by nanoscale and quantitative analyses. *Nano Energy* 67:104201. <https://doi.org/10.1016/j.nanoen.2019.104201>
 30. Khelifi S et al (2010) Characterization of flexible thin film CIGSe solar cells grown on different metallic foil substrates. *Energy Procedia* 2(1):109–117. <https://doi.org/10.1016/j.egypro.2010.07.017>
 31. Liang X et al (2016) Substrate temperature optimization for Cu(In, Ga)Se₂ solar cells on flexible stainless steels. *Appl Surf Sci* 368:464–469. <https://doi.org/10.1016/j.apsusc.2016.02.003>
 32. Zortea L et al (2018) Cu(In, Ga)Se₂ solar cells on low cost mild steel substrates. *Sol Energy* 175:25–30. <https://doi.org/10.1016/j.solener.2017.12.057>
 33. Bae D, Kwon S, Oh J, Kim WK, Park H (2013) Investigation of Al₂O₃ diffusion barrier layer fabricated by atomic layer deposition for flexible Cu (In, Ga) Se₂ solar cells. *Renew Energy* 55:62–68. <https://doi.org/10.1016/j.renene.2012.12.024>
 34. Eisenbarth T, Caballero R, Kaufmann CA, Eicke A, Unold T (2012) Influence of iron on defect concentrations and device performance for Cu(In, Ga)Se₂ solar cells on stainless steel substrates. *Prog Photovolt Res Appl* 20(5):568–574. <https://doi.org/10.1002/pip.2260>
 35. Chen Z et al (2019) Single-crystal MAPbI₃ perovskite solar cells exceeding 21% power conversion efficiency. *ACS Energy Lett* 4(6):1258–1259. <https://doi.org/10.1021/acsenerylett.9b00847>
 36. Zhang Y et al (2020) Achieving reproducible and high-efficiency (> 21%) perovskite solar cells with a presynthesized FAPbI₃ powder. *ACS Energy Lett* 5(2):360–366. <https://doi.org/10.1021/acsenerylett.9b02348>
 37. Theelen M et al (2017) Determination of the temperature dependency of the electrical parameters of CIGS solar cells. *J Renew Sustain Energy* 9(2):021205. <https://doi.org/10.1063/1.4979963>
 38. Daoudia AK, El Hassouani Y, Benami A (2016) Investigation of the effect of thickness, band gap and temperature on the efficiency of CIGS solar cells through SCAPS-1D. *Int J Eng Tech Res* 6:71
 39. Hu C, White RM (1983) *Solar cells*. McGraw-Hill, New York, p 21
 40. Nell ME, Barnett AM (1987) The spectral p-n junction model for tandem solar-cell design. *IEEE Trans Electron Devices* 34(2):257–266. <https://doi.org/10.1109/T-ED.1987.22916>
 41. Dimmler B, Powalla M, Schaeffler R (2005) CIS solar modules: pilot production at Wuerth Solar, pp 189–194
 42. Zhang L, Liu F-f, Li F-y, He Q, Li B-z, Li C-j (2012) Structural, optical and electrical properties of low-temperature deposition Cu(In_xGa_{1-x})Se₂ thin films. *Sol Energy Mater Sol Cells* 99:356–361. <https://doi.org/10.1016/j.solmat.2012.01.002>
 43. Reinhard P et al (2013) Review of progress toward 20% efficiency flexible CIGS solar cells and manufacturing issues of solar modules. *IEEE J Photovolt* 3(1):572–580
 44. Zhang L, He Q, Jiang W-L, Liu F-F, Li C-J, Sun Y (2009) Effects of substrate temperature on the structural and electrical properties of Cu(In, Ga)Se₂ thin films. *Sol Energy Mater Sol Cells* 93(1):114–118. <https://doi.org/10.1016/j.solmat.2008.09.002>
 45. Kodigala SR (2010) Chapter 8—Cu(In_{1-x}Ga_x)Se₂ and CuIn(S_{e1-x}S_x)₂ thin film solar cells. In: Kodigala SR (ed) *Thin films and nanostructures*, vol 35. Academic Press, New York, pp 505–679
 46. Lammer M, Klemm U, Powalla M (2001) Sodium co-evaporation for low temperature Cu(In, Ga)Se₂ deposition. *Thin Solid Films* 387(1):33–36. [https://doi.org/10.1016/S0040-6090\(00\)01712-0](https://doi.org/10.1016/S0040-6090(00)01712-0)
 47. Wang H et al (2010) Effect of substrate temperature on the structural and electrical properties of CIGS films based on the one-stage co-evaporation process. *Semicond Sci Technol* 25:055007. <https://doi.org/10.1088/0268-1242/25/5/055007>
 48. Yang ZY, Wang LD, Song RX, Zhang DX, Fei WD (2015) Effects of substrate temperature on the properties of Cu(In, Ga)Se₂ thin films prepared by sputtering from a quaternary target. *Adv Mater Res* 1061–1062:209–214. <https://doi.org/10.4028/www.scientific.net/AMR.1061-1062.209>
 49. Chirilă A et al (2011) Cu(In, Ga)Se₂ solar cell grown on flexible polymer substrate with efficiency exceeding 17%. *Prog Photovolt Res Appl* 19(5):560–564. <https://doi.org/10.1002/pip.1077>

50. Zhang W et al (2017) Cu(In, Ga)Se₂ thin film solar cells grown at low temperatures. *Solid-State Electronics* 132:57–63. <https://doi.org/10.1016/j.sse.2017.03.003>
51. Gloeckler M, Sites JR, Metzger WK (2005) Grain-boundary recombination in Cu(In, Ga)Se₂ solar cells. *J Appl Phys* 98(11):113704. <https://doi.org/10.1063/1.2133906>
52. Saliba M et al (2016) Incorporation of rubidium cations into perovskite solar cells improves photovoltaic performance. *Science* 354(6309):206. <https://doi.org/10.1126/science.aah5557>
53. Saliba M et al (2016) A molecularly engineered hole-transporting material for efficient perovskite solar cells. *Nat Energy* 1(2):15017. <https://doi.org/10.1038/nenergy.2015.17>
54. Saliba M et al (2016) Cesium-containing triple cation perovskite solar cells: improved stability, reproducibility and high efficiency. *Energy Environ Sci* 9(6):1989–1997. <https://doi.org/10.1039/c5ee03874j>
55. Leguy AM et al (2015) Reversible hydration of CH₃NH₃PbI₃ in films, single crystals, and solar cells. *Chem. Mater.* 27(9):3397–3407. <https://doi.org/10.1021/acs.chemmater.5b00660>
56. Cuce E, Cuce PM, Bali T (2013) An experimental analysis of illumination intensity and temperature dependency of photovoltaic cell parameters. *Appl Energy* 111:374–382. <https://doi.org/10.1016/j.apenergy.2013.05.025>
57. Shockley W, Queisser HJ (1961) Detailed balance limit of efficiency of p–n junction solar cells. *J Appl Phys* 32(3):510–519. <https://doi.org/10.1063/1.1736034>
58. Eperon GE, Stranks SD, Menelaou C, Johnston MB, Herz LM, Snaith HJ (2014) Formamidinium lead trihalide: a broadly tunable perovskite for efficient planar heterojunction solar cells. *Energy Environ Sci* 7(3):982–988. <https://doi.org/10.1039/c3ee43822h>
59. Lv S et al (2014) One-step, solution-processed formamidinium lead trihalide (FAPbI_{3–x}Cl_x) for mesoscopic perovskite–polymer solar cells. *Phys Chem Chem Phys* 16(36):19206–19211. <https://doi.org/10.1039/c4cp02113d>
60. Shao Y et al (2016) Grain boundary dominated ion migration in polycrystalline organic–inorganic halide perovskite films. *Energy Environ Sci* 9(5):1752–1759. <https://doi.org/10.1039/c6ee00413j>
61. Zou Y, Holmes RJ (2016) Temperature-dependent bias poling and hysteresis in planar organo-metal halide perovskite photovoltaic cells. *Adv Energy Mater* 6(7):1501994. <https://doi.org/10.1002/aenm.201501994>
62. Leong WL et al (2016) Identifying fundamental limitations in halide perovskite solar cells. *Adv Mater* 28(12):2439–2445. <https://doi.org/10.1002/adma.201505480>
63. Zhang H, Qiao X, Shen Y, Wang M (2015) Effect of temperature on the efficiency of organometallic perovskite solar cells. *J Energy Chem* 24(6):729–735. <https://doi.org/10.1016/j.jechem.2015.10.007>
64. Wang M, Yim W-L, Liao P, Shen Y (2017) Temperature dependent characteristics of perovskite solar cells. *ChemistrySelect* 2(16):4469–4477. <https://doi.org/10.1002/slct.201700776>
65. Aharon S, Dymshits A, Rotem A, Etgar L (2015) Temperature dependence of hole conductor free formamidinium lead iodide perovskite based solar cells. *J Mater Chem A* 3(17):9171–9178. <https://doi.org/10.1039/c4ta05149a>
66. Dualeh A, Moehl T, Nazeeruddin MK, Grätzel M (2013) Temperature dependence of transport properties of spiro-MeOTAD as a hole transport material in solid-state dye-sensitized solar cells. *ACS Nano* 7(3):2292–2301. <https://doi.org/10.1021/nn4005473>
67. Tress W et al (2019) Performance of perovskite solar cells under simulated temperature-illumination real-world operating conditions. *Nat Energy* 4(7):568–574. <https://doi.org/10.1038/s41560-019-0400-8>
68. Chen HW, Sakai N, Ikegami M, Miyasaka T (2015) Emergence of hysteresis and transient ferroelectric response in organo-lead halide perovskite solar cells. *J Phys Chem Lett* 6(1):164–169. <https://doi.org/10.1021/jz502429u>
69. Conings B et al (2015) Intrinsic thermal instability of methylammonium lead trihalide perovskite. *Adv Energy Mater* 5(15):1500477. <https://doi.org/10.1002/aenm.201500477>
70. Lee JW, Kim SG, Yang JM, Yang Y, Park NG (2019) Verification and mitigation of ion migration in perovskite solar cells. *APL Mater* 7(4):041111. <https://doi.org/10.1063/1.5085643>
71. Lee JW, Kim DH, Kim HS, Seo SW, Cho SM, Park NG (2015) Formamidinium and cesium hybridization for photo- and moisture-stable perovskite solar cell. *Adv Energy Mater* 5(20):1501310. <https://doi.org/10.1002/aenm.201501310>
72. Wali Q, Elumalai NK, Iqbal Y, Uddin A, Jose R (2018) Tandem perovskite solar cells. *Renew Sustain Energy Rev* 84:89–110. <https://doi.org/10.1016/j.rser.2018.01.005>
73. Jošt M (2020) Perovskite solar cells go outdoors: field testing and temperature effects on energy yield. *Adv Energy Mater.* <https://doi.org/10.1002/aenm.202000454>
74. Checharoen R, Rolston N, Harwood D, Bush KA, Dauskardt RH, McGehee MD (2018) Design and understanding of encapsulated perovskite solar cells to withstand temperature cycling. *Energy Environ Sci* 11(1):144–150. <https://doi.org/10.1039/c7ee02564e>
75. Domanski K, Alharbi EA, Hagfeldt A, Grätzel M, Tress W (2018) Systematic investigation of the impact of operation conditions on the degradation behaviour of perovskite solar cells. *Nat Energy* 3(1):61–67. <https://doi.org/10.1038/s41560-017-0060-5>
76. Schwenzer JA et al (2018) Temperature variation-induced performance decline of perovskite solar cells. *ACS Appl Mater Interfaces* 10(19):16390–16399. <https://doi.org/10.1021/acsami.8b01033>
77. McMeekin DP et al (2016) A mixed-cation lead mixed-halide perovskite absorber for tandem solar cells. *Science* 351(6269):151. <https://doi.org/10.1126/science.aad5845>

Publisher's Note Springer Nature remains neutral with regard to jurisdictional claims in published maps and institutional affiliations.